# Impact of Phosphorylation on Structure and Thermodynamics of the Interaction between the N-terminal Domain of Enzyme I and the Histidine Phosphocarrier Protein of the Bacterial Phosphotransferase System*

**Jeong-Yong Suh, Mengli Cai, and G. Marius Clore**[1]
*From the Laboratory of Chemical Physics, NIDDK, National Institutes of Health, Bethesda, Maryland 20892*

The structural and thermodynamic impact of phosphorylation on the interaction of the N-terminal domain of enzyme I (EIN) and the histidine phosphocarrier protein (HPr), the two common components of all branches of the bacterial phosphotransferase system, have been examined using NMR spectroscopy and isothermal titration calorimetry. His-189 is located at the interface of the α and αβ domains of EIN, resulting in rather widespread chemical shift perturbation upon phosphorylation, in contrast to the highly localized perturbations seen for HPr, where His-15 is fully exposed to solvent. Residual dipolar coupling measurements, however, demonstrate unambiguously that no significant changes in backbone conformation of either protein occur upon phosphorylation: for EIN, the relative orientation of the α and αβ domains remains unchanged; for HPr, the backbone $\phi/\psi$ torsion angles of the active site residues are unperturbed within experimental error. His → Glu/Asp mutations of the active site histidines designed to mimic the phosphorylated states reveal binding equilibria that favor phosphoryl transfer from EIN to HPr. Although binding of phospho-EIN to phospho-HPr is reduced by a factor of ~21 relative to the unphosphorylated complex, residual dipolar coupling measurements reveal that the structures of the unphosphorylated and biphosphorylated complexes are the same. Hence, the phosphorylation states of EIN and HPr shift the binding equilibria predominantly by modulating intermolecular electrostatic interactions without altering either the backbone scaffold or binding interface. This facilitates highly efficient phosphoryl transfer between EIN and HPr, which is estimated to occur at a rate of ~850 s$^{-1}$ from exchange spectroscopy.

The bacterial phosphotransferase system (PTS)[2] couples sequential phosphoryl transfer via a series of biomolecular protein-protein interactions to active sugar transport across the membrane (1–4). In addition, the phosphorylation state of individual components of the PTS act as switches in the regulation of diverse cellular processes, including transcription, chemotaxis, and glycolysis (4). The first two proteins in the PTS, enzyme I, and the histidine phosphocarrier protein (HPr) are common to all branches, whereas subsequent phosphorylation transfer steps involve sugar-specific permeases, also known as enzymes II. The initial step in the PTS involves autophosphorylation of enzyme I (EI) at the Nε2 atom of His-189 by phosphoenolpyruvate (PEP) (5, 6). Autophosphorylation requires the presence of the C-terminal domain of EI (EIC), but reversible phosphoryl transfer from EI to the Nδ1 atom of His-15 of HPr (7) only requires the N-terminal domain of EI, EIN (8, 9). The phosphoryl group is subsequently transferred from HPr through a sequence of two cytoplasmic enzyme II components, A and B, to the incoming sugar bound to the cytoplasmic side of the membrane-bound sugar permease (1–4).

The phosphotransfer reactions within the PTS are reversible (4). In the resting state (in the absence of external sugar), the high phosphotransfer potential of PEP maintains the cellular PTS proteins in a fully phosphorylated state (10, 11). Upon sugar translocation and concomitant phosphorylation of the incoming sugar, the sequential phosphoryl transfer cascade is resumed. Little is known of how protein-protein interactions within the PTS are affected by phosphorylation.

In this paper, we examine the effect of phosphorylation on the structures of EIN, HPr, and the biphosphorylated EIN·HPr complex. We show using residual dipolar coupling (RDC) measurements (12, 13) that no significant backbone perturbation is observed upon phosphorylation of either EIN or HPr and that the relative orientation of EIN and HPr in a fully biphosphorylated complex is the same as that in the unphosphorylated complex. However, the equilibrium constants for the interaction between EIN and HPr are significantly affected by phosphorylation state, as measured by isothermal titration calorimetry (ITC). Finally, we determine the approximate overall rate constant for phosphoryl transfer between EIN and HPr by qualitative interpretation of cross-peak line widths in $^1$H-$^{15}$N

[1] To whom correspondence should be addressed: Laboratory of Chemical Physics, Bldg. 5, NIDDK, National Institutes of Health, Bethesda, MD 20892-0520. Tel.: 301-496-0782; Fax: 301-496-025; E-mail: mariusc@mail.nih.gov.

[2] The abbreviations used are: PTS, bacterial phosphotransferase system; HPr, histidine phosphocarrier protein; EI, enzyme I; EIN, N-terminal domain of enzyme I (residues 1–249); EIC, C-terminal domain of enzyme I (phosphoenolpyruvate binding domain); PEP, phosphoenolpyruvate; HSQC, heteronuclear single quantum coherence; RDC, residual dipolar coupling; PEG, polyethylene glycol; ITC, isothermal titration calorimetry; SVD, singular value decomposition.

correlation spectra recorded during the course of active phosphoryl transfer.

## EXPERIMENTAL PROCEDURES

*Cloning, Expression, and Purification of EIN and HPr*—EIN (residues 1–249) and HPr (residues 1–85) were cloned into a pET15b vector (Novagen) without tags. The active site His-189 of EIN and His-15 of HPr were mutated to Glu or Asp using the QuikChange kit (Stratagene), and the new constructs were verified by DNA sequencing. The plasmids were introduced into *Escherichia coli* strain BL21star(DE3) (Invitrogen) cells for expression. Cells were grown in either Luria Bertini or minimal medium (with $^{15}NH_4Cl$ and/or $^{13}C_6$-glucose as the sole nitrogen or carbon source, respectively) in $H_2O$ or $D_2O$, induced with 1 mM isopropyl-D-thiogalactopyranoside at an $A_{600}$ of 0.8, and harvested by centrifugation after 4 h of induction. The cell pellet was resuspended in 50 ml (per liter of culture) of 50 mM Tris, pH 8.0, 200 mM NaCl, 2 mM dithiothreitol, and 1 mM phenylmethylsulfonyl fluoride. The suspension was lysed by three passages through a microfluidizer and centrifuged at $70,000 \times g$ for 20 min. The supernatant fraction was filtered and loaded onto a DEAE anion exchange column (20 ml; GE Healthcare), and the protein was eluted with a 400-ml gradient of 1 M NaCl. The fractions containing the protein were confirmed by SDS-polyacrylamide gel electrophoresis and purified by gel filtration on a Sephadex-75 column (GE Healthcare) equilibrated with 20 mM Tris, pH 7.4, 200 mM NaCl, and 0.01% (w/v) sodium azide. Relevant fractions were dialyzed against 20 mM Tris, pH 7.4, and finally purified on a monoQ anion exchange column (GE Healthcare). NMR samples were prepared in 20 mM Tris buffer, pH 7.4, and 10% $D_2O$ (v/v). For protein phosphorylation, 1% (c/c) EI (prepared as described previously (14)) and HPr were added to the sample in conjunction with 1 mM $MgCl_2$ and 50 mM PEP.

*NMR Spectroscopy*—NMR spectra were recorded at 37 °C on Bruker 600 MHz spectrometers (DMX or DRX) equipped with either a z-shielded gradient triple resonance cryoprobe or, for $^{31}P$ NMR, an x,y,z-shielded gradient quadruple resonance probe. Spectra were processed using NMRPipe (15) and analyzed using the program PIPP (16) or NMRView (17). Sequential assignments of phosphorylated EIN and phosphorylated HPr were performed using three-dimensional triple resonance through-bond scalar correlation experiments (HNCACB and CBCA(CO)NH (18, 19).

$^1D_{NH}$ RDCs were measured by taking the difference in $^1J_{NH}$ scalar couplings in aligned and isotropic media (12). The alignment media employed were phage *pf1* (11 mg/ml; ASLA Biotech) (20, 21) for phosphorylated EIN and the biphosphorylated EIN·HPr complex, and 5% C12E5 polyethylene glycol (PEG)/*n*-hexanol (Fluka) (22) for phosphorylated HPr. Singular value decomposition (SVD) analysis of RDCs (12, 13) was carried out using Xplor-NIH (23).

For titration experiments, a 1 mM concentration of one protein was titrated with the other protein in either phosphorylated or unphosphorylated states. For titration experiments involving the phosphorylated states, 1% (c/c) EI, 5 mM $MgCl_2$, and 50 mM PEP were used to keep the proteins fully phosphorylated. Time course experiments were carried out using 1 mM
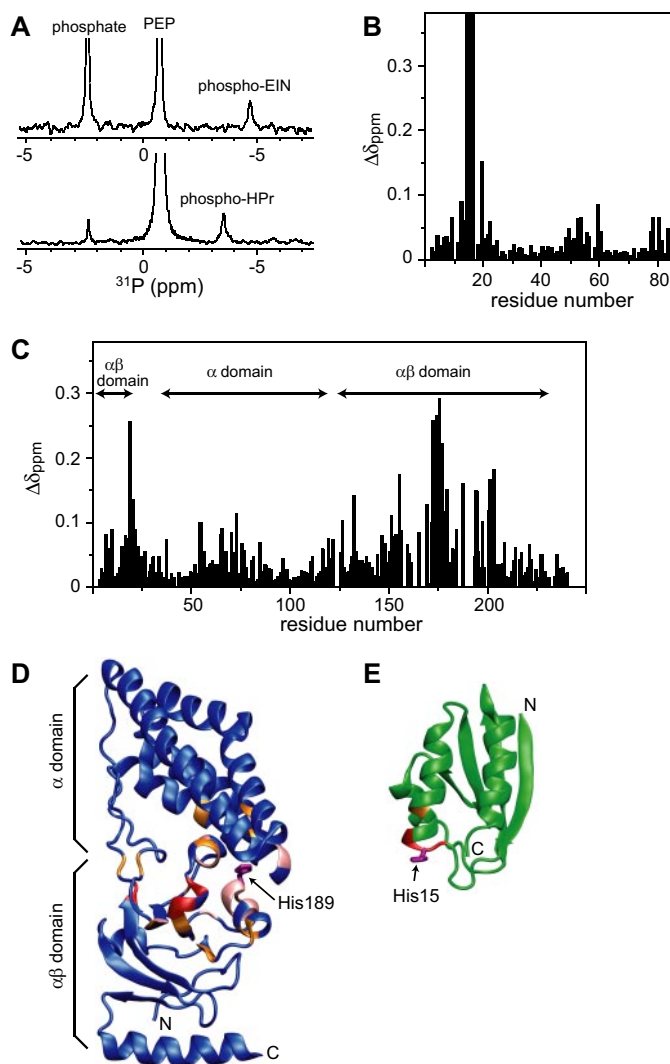


FIGURE 1. **Impact of phosphorylation on the NMR spectra of EIN and HPr.** *A*, $^{31}P$ NMR spectra of phospho-EIN (*top*) and phospho-HPr (*bottom*). Shown is the weighted average $^1H_N/^{15}N$ chemical shift perturbation ($\Delta\delta_{ave} = ([(\Delta\delta_{HN})^2 + (\Delta\delta_N)^2/25]/2)^{1/2}$) as a function of residue number upon phosphorylation of HPr (*B*) and EIN (*C*). Shown is mapping of phosphorylation-induced chemical shift perturbation on *ribbon diagrams* of the three-dimensional structures of unphosphorylated EIN (*D*) and HPr (*E*) (from Protein Data Bank code 3EZA) (28) with residues exhibiting $\Delta\delta_{ave} > 0.2$ colored in *red* and residues with $0.1 < \Delta\delta_{ave} \leq 0.2$ in *yellow*. Residues that could not be unambiguously assigned due to spectral overlap or line broadening are colored in *lilac*. The active site histidine side chains are show in *magenta*.

$^{15}N$-labeled EIN and 1 mM unlabeled HPr in the presence of 10 μM EI, 5 mM $MgCl_2$, and 20 mM PEP, and $^{15}N$-$^1H$ heteronuclear single quantum coherence (HSQC) spectra were collected at 30-min intervals until both proteins were completely dephosphorylated.

*Isothermal Titration Calorimetry*—ITC was performed using a VP-ITC calorimeter (Microcal Inc.). 0.1 mM EIN was placed in the cell and titrated with 1 mM HPr in the syringe at 37 °C for wild-type and mutant proteins. For titrations involving the phosphorylated states, 0.15 mM EIN and 2 mM HPr were used with 1% (c/c) of enzymes (EI and HPr), 1 mM $MgCl_2$, and 20 mM PEP present in the cell and the syringe to maintain both EIN and HPr in a fully phosphorylated state during the course of the titration. Analysis of the data was performed using the Origin software provided with the instrument. When phosphorylated
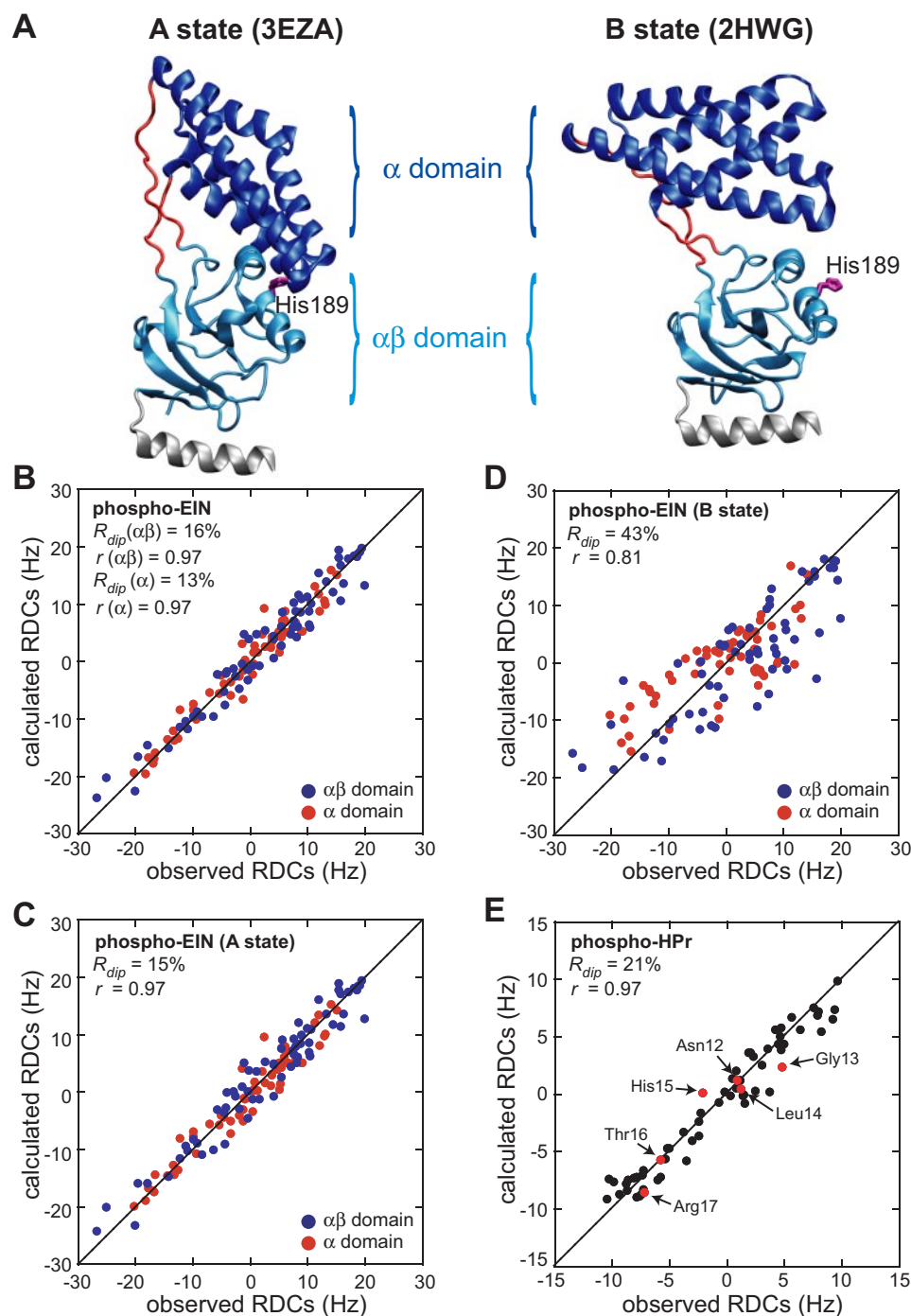
FIGURE 2. **RDC analysis of the impact of phosphorylation on the backbone structure of EIN and HPr.** *A*, *ribbon diagrams* of the structure of the A (*left*) and B (*right*) states of EIN. The A state refers to the orientation of the $\alpha$ and $\alpha\beta$ domains observed in the NMR (29) and x-ray (30) structures of free EIN and the NMR structure of the unphosphorylated EIN·HPr complex (28) (Protein Data Bank code 3EZA). The B state refers to the orientation of the $\alpha$ and $\alpha\beta$ domains observed in the x-ray structure of full-length phosphorylated EI (31) (Protein Data Bank code 2HWG). The $\alpha\beta$ domains of the A and B states are shown in identical views. The $\alpha$ domain is in *dark blue*, the $\alpha\beta$ domain in *light blue*, the linkers between the $\alpha$ and $\alpha\beta$ domains in *red*, the linker helix that connects EIN to EIC in *gray*, and His-189 in *magenta*. Shown is a comparison of observed and calculated $^1D_{NH}$ RDCs obtained by SVD with individual fits (*B*) and a global fit (*C*) to the NMR coordinates of the $\alpha$ (*red*) and $\alpha\beta$ (*blue*) domains of unphosphorylated EIN (A state; 3EZA) (28). *D*, comparison of observed and calculated $^1D_{NH}$ RDCs with a global fit to the B state of EIN. The coordinates for the B state used in the analysis comprise the NMR coordinates of the $\alpha$ and $\alpha\beta$ domains in the B state orientation obtained by best fitting the domains individually onto their respective domains of the x-ray coordinates of phosphorylated EI (Protein Data Bank code 2HWG). *E*, comparison of observed and calculated $^1D_{NH}$ RDCs for phospho-HPr using the 1.6 Å resolution x-ray structure of unphosphorylated HPr (Protein Data Bank code 1POH) (37). The RDCs for phospho-EIN were measured in an alignment medium of phage *pf1*, and those for phospho-HPR were measured in an alignment medium of 5% PEG/hexanol. The values of the correlation coefficients (*r*) and RDC R-factors ($R_{dip}$) are shown. The five parameters describing the orientation and magnitude of the RDC alignment tensors are given in Table 1.

proteins were titrated, significant base-line drift was observed due to continuous dephosphorylation and rephosphorylation in the cell and corrected prior to analysis using the reference titration of phosphorylated HPr into the cell in the absence of EIN.

## RESULTS AND DISCUSSION

*Structures of Phosphorylated EIN and HPr*—EIN and HPr were enzymatically phosphorylated using catalytic amounts of EI, HPr, and a large excess of PEP. EIN is phosphorylated at the N$\epsilon$2 atom of His-189 (5, 6), and HPr is phosphorylated at the N$\delta$1 atom of His-15 (7, 24–27). Since the phosphoryl group on the active site histidines of both proteins is labile and continually lost to buffer by acid-catalyzed hydrolysis with a $t_{1/2}$ of ~20 min at pH 7.4, PEP is continually consumed, and inorganic phosphorus is generated. Therefore, full protein phosphorylation was confirmed after completion of NMR structure-based experiments (*e.g.* measurement of RDCs) by either $^1H$-$^{15}N$ HSQC spectroscopy or one-dimensional $^{31}P$ NMR spectroscopy (Fig. 1*A*). The $^{31}P$ NMR signal of phospho-EIN resonates at −4.82 ppm (referenced to phosphoric acid at 0 ppm), consistent with the $^{31}P$ shift of −4.73 ppm for N$\epsilon$-phosphohistidine at pH 7.4 (24). The $^{31}P$ signal of phospho-HPr resonates at −3.63 ppm, which is ~2 ppm downfield relative to that of N$\delta$-phosphohistidine (−5.55 ppm at pH 7.4) (25). This is due to hydrogen bonding between the phosphoryl group and the backbone amide groups of Thr-16 and Arg-17, as well as the hydroxyl group of Thr-16, in the active site (26–28); upon pH-induced unfolding of HPr, the difference in $^{31}P$ chemical shift between phospho-HPr and N$\delta$-phosphohistidine disappears (24, 25).

Chemical shift perturbation of the $^1H$-$^{15}N$ HSQC spectrum of EIN is quite extensive upon phosphorylation, involving both the $\alpha$ (residues 33–143) and $\alpha\beta$ (residues 1–20 and 148–230) domains (Fig. 1*C*), con-

sistent with previously preliminary results reported for partially phosphorylated EIN (6). Given the location of His-189, the largest perturbations involve residues located at the interface between the $\alpha$ and $\alpha/\beta$ domains (Fig. 1D). The chemical shift perturbations, however, are not due to reorientation of the $\alpha$ and $\alpha\beta$ domains upon phosphorylation (see below) but rather to electronic effects arising from the presence of the phosphoryl group as well as ring current effects due to a change in the $\chi_2$ angle of His-189 from the $g^+$ to $g^-$ rotameric state that breaks the hydrogen bond between the N$\epsilon$2 atom of His-189 and the hydroxyl group of Thr-69, thereby rendering the N$\epsilon$2 atom accessible to the incoming phosphoryl group (28–30).

Recently, a 2.7 Å resolution crystal structure was published for intact phosphorylated EI obtained by mixing the protein with PEP followed by quenching of the autophosphorylation reaction by the EI inhibitor oxalate (31) (Protein Data Bank code 2HWG). In the crystal structure of phosphorylated EI, there is a large ~65° reorientation of the $\alpha$ and $\alpha\beta$ subdomains within the EIN domain (31) relative to that observed in the structure of isolated EIN, both free in solution (29) and in the crystal state (30), as well as complexed with HPr (28). As a consequence of domain reorientation, the phosphoryl group on His-189 (located in the $\alpha\beta$ subdomain) is buried in the PEP binding site on the EIC domain (31) and can no longer interact with His-15 of HPr. Further, although the HPr binding site on the $\alpha$ subdomain is still fully accessible to HPr, the distance between His-189 of phosphorylated EI and His-15 of HPr (with HPr docked to its binding site on the $\alpha$ subdomain) is 30 Å and therefore incompatible with downstream phosphoryl transfer from EI to HPr (31). It was therefore proposed (31) that the crystal structure of phosphorylated EI corresponds to a trapped intermediate just after auto-phosphorylation by PEP but prior to the postulated conformational transitions involving swiveling and hinge rotation of both EIC and the $\alpha$ subdomain required to bring His-189 in close proximity to His-15 of HPr, as observed in the structure of the EIN·HPr complex (28). In this paper, we refer to the orientation of the $\alpha$ and $\alpha\beta$ subdomains observed in the free and complexed structures of EIN (28–30) as the A state (Fig. 2A, *left*), and we refer to that observed in the crystal structure of phosphorylated EI as the B state (Fig. 2A, *right*).

To assess whether domain reorientation of the $\alpha$ and $\alpha\beta$ domains of EIN occurs upon phosphorylation of EIN alone, we proceeded to measure backbone amide RDCs on phospho-EIN in a liquid crystalline medium of phage *pf1*. RDCs of fixed bond vectors, such as the backbone N–H bond vector, are dependent on the orientation of the bond vectors relative to the alignment tensor and provide a very sensitive indicator of changes in relative domain orientations (12, 13). The magnitude and orientation of the alignment tensors obtained by SVD to obtain a best fit between the observed RDCs and those calculated from the atomic coordinates of EIN (taken from the NMR structure of the EIN·HPr complex, Protein Data Bank code 3EZA) (28) are the same within experimental error using the coordinates of the $\alpha$ and $\alpha\beta$ domains individually or together (Table 1 and Fig. 2, B and C). In addition, the RDC R-factor ($R_{dip}$) (32) obtained from the global fit (15%) is comparable with that obtained from the individual fits to the $\alpha$ ($R_{dip}$ = 13%) and $\alpha\beta$ ($R_{dip}$ = 16%)

## TABLE 1
### SVD analysis of $^1D_{NH}$ RDCs measured for phospho-EIN

The alignment tensor is described by five parameters: three Euler angles, which describe the orientation of the tensor in the atomic coordinate frame, the magnitude of the principal component of the tensor ($D_a^{NH}$), and the rhombicity ($\eta$). The coordinate frame for the $\alpha\beta$ domain in all three fits is the same. The analysis presented in the table shows the values describing the alignment tensor obtained from analysis of the $\alpha\beta$ (residues 2–20 and 148–230) and $\alpha$ (residues 33–143) domains individually and together (29, 30).

| | Number of RDCs | Euler angles | | | $D_a^{NH}$ | $\eta$ | RDC R-factor[a] |
|---|---|---|---|---|---|---|---|
| | | $\varphi$ | $\theta$ | $\psi$ | | | |
| | | *degrees* | | | *Hz* | | *%* |
| **A state (3EZA NMR coordinates)[b]** | | | | | | | |
| Individual fits[b] | | | | | | | |
| $\alpha\beta$ domain | 62 | 161 | 273 | 13 | −12.4 | 0.42 | 15.6 |
| $\alpha$ domain | 62 | 155 | 273 | 7 | −12.4 | 0.39 | 12.5 |
| Global fit | 124 | 158 | 272 | 11 | −12.5 | 0.39 | 15.1 |
| **B state (2HWG orientation with NMR coordinates of $\alpha$ and $\alpha\beta$ domains)[c]** | | | | | | | |
| Individual fits | | | | | | | |
| $\alpha\beta$ domain | 62 | 161 | 273 | 14 | −12.4 | 0.42 | 15.6 |
| $\alpha$ domain | 62 | 35 | 70 | 153 | −12.4 | 0.39 | 12.5 |
| Global fit | 124 | 182 | 290 | 28 | −10.0 | 0.55 | 43.4 |
| **B state (2HWG x-ray coordinates)[c]** | | | | | | | |
| Individual fits | | | | | | | |
| $\alpha\beta$ domain | 62 | 168 | 283 | 158 | −11.4 | 0.37 | 33.5 |
| $\alpha$ domain | 62 | 37 | 63 | 160 | −9.8 | 0.30 | 29.4 |
| Global fit | 124 | 183 | 295 | 30 | −9.5 | 0.53 | 46.7 |

[a] The RDC R-factor, which scales between 0 and 100%, is defined as the ratio of the root mean square deviation between observed and calculated values to the expected root mean square deviation if the vectors were randomly distributed, given by $[2D_a^2(4 + 3\eta^2)/5]^{1/2}$ (32).

[b] The A state refers to the orientation of the $\alpha$ and $\alpha\beta$ domains in the coordinates of the unphosphorylated EIN structure taken from the structure of the unphosphorylated EIN·HPr complex determined by NMR (Protein Data Bank accession code 3EZA) (28). The three alignment tensors and the RDC R-fctors are identical within experimental error, indicating that the relative orientation of the $\alpha$ and $\alpha\beta$ domains in phospho-EIN is the same as that in unphosphorylated EIN.

[c] The B state refers to the orientation of the $\alpha$ and $\alpha\beta$ domains in the x-ray structure of full-length phosphorylated EI (31). Analysis of the B state is presented using the x-ray coordinates of phosphorylated EI (Protein Data Bank code 2HWG) as well as the NMR coordinates of the $\alpha$ and $\alpha\beta$ domains taken from 3EZA best fitted to the respective domains in the 2HWG structure. The Ca atomic root mean square difference between the NMR and x-ray coordinates of the $\alpha$ and $\alpha\beta$ domains is 1.4–1.5 Å for each domain. The higher dipolar coupling R-factors for the fits of the individual domains to the 2HWG coordinates reflects the relatively low resolution (2.7 Å) of the x-ray structure and hence the reduced accuracy and increased uncertainty of the N–H bond vector orientations. In both cases, the orientations of the alignment tensors for the $\alpha$ and $\alpha\beta$ domains obtained from the individual fits are different, and the global fit is poor. These results prove that the orientation of the $\alpha$ and $\alpha\beta$ domains in phosphorylated EIN does not correspond to that of the B state seen in the x-ray structure of full-length phosphorylated EI (Protein Data Bank code 2HWG).

domains. (Note that these $R_{dip}$ values are consistent with those expected for 1.5–2 Å resolution crystal structures (33–36).) In contrast, the measured RDC data are not consistent with the B state conformation seen in the crystal structure of phosphorylated EI (Fig. 2D and Table 1). The orientations of the alignment tensors are different for the $\alpha$ and $\alpha\beta$ domains (Table 1), and the global fit is very poor ($R_{dip}$ = 43%) (Fig. 2D). (Note that the coordinates of the $\alpha$ and $\alpha\beta$ domains used in Fig. 2 are taken from the NMR structure of the EIN·HPr complex in either the A or B state orientations. The latter are simply obtained by best fitting the coordinates of the two domains individually to the coordinates of their respective domains in the x-ray structure of phosphorylated EI. If the x-ray coordinates of phosphorylated EI are used, the RDC R-factors for the fits to the individual $\alpha$ and $\alpha\beta$ domains are significantly worse than those for the NMR coordinates, reflecting the relatively low 2.7 Å resolution of the

crystal structure and hence the reduced accuracy and increased uncertainty of the N–H bond vector orientations; however, the orientation of the alignment tensors for the $\alpha$ and $\alpha\beta$ domain remain different, and the RDC $R$-factor for the global fit is significantly worse than that for the individual fits (*cf.* Table 1). Thus, one can conclude unambiguously that the orientation of the $\alpha$ and $\alpha\beta$ domains in phospho-EIN corresponds to that of the A state conformation seen in unphosphorylated EIN, both free (29, 30) and complexed to HPr (28), and that the B state observed in the crystal structure of phosphorylated EI (31) represents an intermediate immediately after phosphoryl transfer from PEP and prior to domain reorientation to yield the A state necessary for subsequent downstream phosphoryl transfer to HPr.

In the case of HPr, His-15 is located at the N terminus of helix $\alpha1$ and is fully exposed to solvent (Fig. 1*E*). Hence, $^1H/^{15}N$ chemical shift perturbations upon phosphorylation are localized to the active site loop (His-15, Thr-16, and Arg-17) and to a lesser degree Ala-20 and Ile-61 (Fig. 1, *B* and *E*). Although earlier NMR work (26, 27), largely based on nuclear Overhauser enhancement measurements, suggested that some significant but localized changes in backbone conformation occur upon phosphorylation, RDC measurements (in a liquid crystalline medium of PEG/hexanol) indicate that there are no significant backbone conformational changes. (Note that phage *pf1* was not used as an alignment medium, since *pf1* interacts too strongly with free HPr to permit RDCs to be measured). Thus, the measured RDCs are in excellent agreement with the 1.6 Å resolution crystal structure of unphosphorylated *E. coli* HPr (Protein Data Bank code 1POH) (37), and no deviations are apparent for the RDCs of the N–H bond vectors of the active site residues extending from Asn-12 to Arg-17 (Fig. 2*C*). The latter observation demonstrates that the $\phi/\psi$ backbone torsion angles of the active site residues are essentially unperturbed upon phosphorylation of HPr.

*Impact of Phosphorylation on Stability of the EIN·HPr Complex*— Equilibrium binding of EIN and HPr in different combinations of phosphorylated or phosphomimetic states
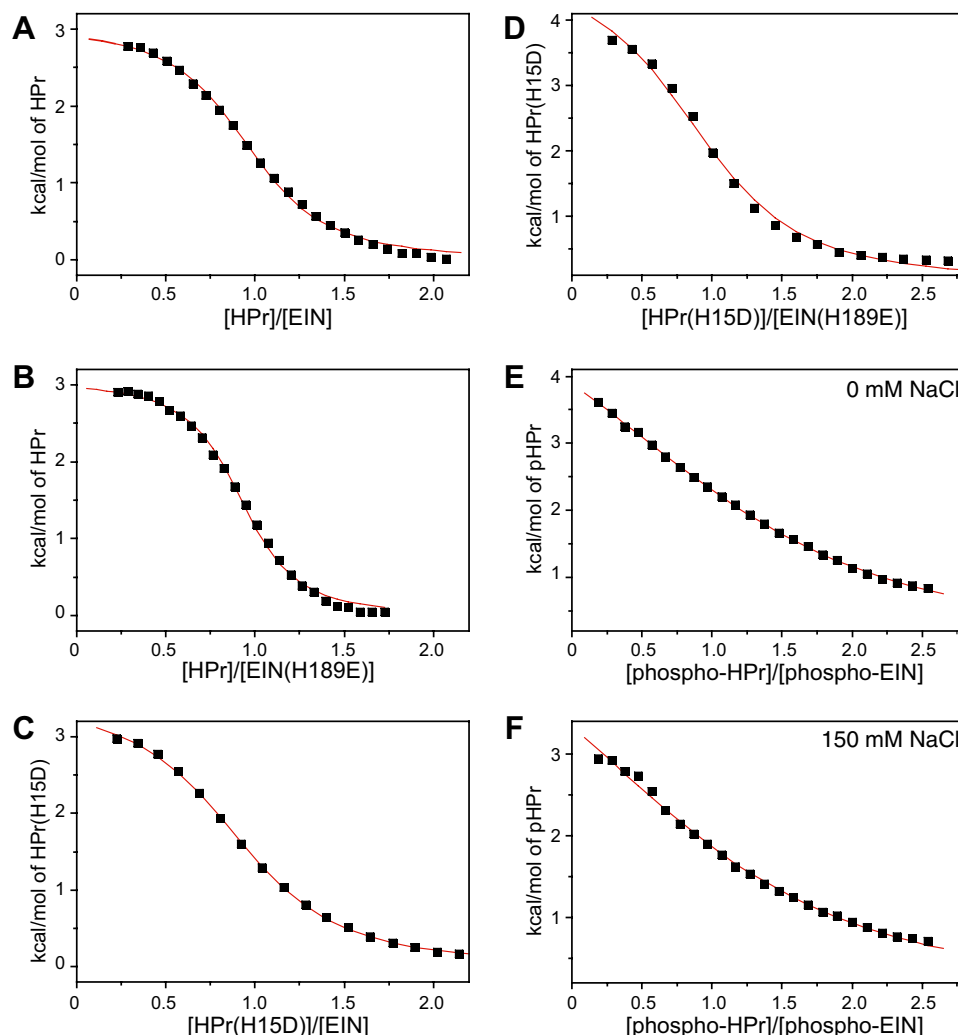


FIGURE 3. **ITC of the interaction of EIN and HPr.** Integrated heats of injection (*solid squares*) and the least squares best fit curves (*red lines*), derived from a simple one-site binding model for the titration between HPr and EIN (*A*), HPr and EIN(H189E) (*B*), HPr(H15D) and EIN (*C*), HPr(H15D) and EIN(H189E) (*D*), and phospho-HPr and phospho-EIN (*E*) in the absence of NaCl. *F*, same as *E* but in the presence of 150 mM NaCl. All titrations were carried out in 20 mM Tris-HCl buffer, pH 7.4, at 37 °C. The equilibrium dissociation constants and thermodynamic parameters derived from the data are given in Table 2.

**TABLE 2**

**Equilibrium dissociation constants ($K_D$), binding free energies ($\Delta G$), binding enthalpies ($\Delta H$), and entropies ($\Delta S$) for the interaction between EIN and HPr in various combinations of unphosphorylated, phosphorylated, and phosphomimetic states**

All titrations were carried out in 20 mM Tris-HCl buffer, pH 7.4, at 37 °C. With the exception of the last entry, titrations were carried out in the absence of NaCl.

| | $K_D$ | $\Delta G$ | $\Delta H$ | $\Delta S$ |
|---|---|---|---|---|
| | $\mu M$ | $kcal\cdot mol^{-1}$ | $kcal\cdot mol^{-1}$ | $cal\cdot mol^{-1}\cdot T^{-1}$ |
| EIN/HPr | 5.1 ± 0.4 | −7.5 ± 0.05 | 3.0 ± 0.05 | 34.0 ± 0.2 |
| EIN(H189E)/HPr | 2.6 ± 0.2 | −7.9 ± 0.05 | 3.0 ± 0.04 | 35.3 ± 0.2 |
| EIN/HPr(H15D) | 10 ± 0.3 | −7.1 ± 0.02 | 3.5 ± 0.03 | 34.2 ± 0.1 |
| EIN(H189E)/HPr(H15D) | 24 ± 4 | −6.6 ± 0.09 | 4.8 ± 0.2 | 36.6 ± 0.8 |
| Phospho-EIN/phospho-HPr | 108 ± 4 | −5.6 ± 0.02 | 5.9 ± 0.1 | 37.1 ± 0.3 |
| Phospho-EIN/phospho-HPr (150 mM NaCl) | 123 ± 13 | −5.6 ± 0.07 | 5.5 ± 0.4 | 35.8 ± 1.3 |

was studied by ITC (Fig. 3). To mimic individual phosphorylated proteins, the active site histidines of EIN and HPr were mutated to Glu and Asp, respectively.

Relative to the unphosphorylated EIN·HPr complex, the EIN(H189E)· HPr complex showed 2-fold stronger binding, whereas the EIN· HPr(H15D) complex displayed 2-fold weaker binding (Table 2 and Fig. 3, *A–C*). This thermodynamic ratio would favor the phosphotransfer reaction from EIN to HPr by a factor of 4.

We also measured the binding of phospho-EIN to phospho-HPr, which is relevant to the situation in the cell when sugar transport by the PTS is inactive. The interaction of EIN(H189E) and HPr(H15D) is 5 times weaker and that between phospho-EIN and phospho-HPr is 21 times weaker than that between unphosphorylated EIN and HPr (Table 2 and Fig. 3, *D* and *E*). In both cases, the increase in $K_D$ can be largely attributed to an unfavorable binding enthalpy, indicating that electrostatic repulsion between the active site residues is mainly responsible for the decreased binding affinity (Table 2). Phosphorylated histidine occupies a larger space than either glutamate or aspartate, accounting for the observation that the binding between the mutant His → Glu/Asp proteins overestimates the binding between actual phosphorylated proteins by a factor of about 4. The interaction between the phosphorylated proteins is much less sensitive to salt concentration than that of the unphosphorylated complex (Table 2 and Fig. 3, *E* and *F*) (38). This can be attributed to a decrease in the favorable contribution of electrostatic interactions to the binding energy as a consequence of charge repulsion between the two phosphoryl groups. Modeling on the basis of the structure of the unphosphorylated EIN·HPr complex (28) suggests that the negative impact of charge repulsion between the two phosphoryl groups, as well as between the two carboxylate groups in the case of the HPr(H189E)·HPr(H15D) complex, may be partially mitigated by water-bridged hydrogen bonds between the two negatively charged groups.

*Overall Structure of the Biphosphorylated EIN·HPr Complex—* We investigated how protein phosphorylation affects the overall structure of the EIN·HPr complex by means of $^1H_N/^{15}N$ chemical shift perturbation and RDC measurements.

Examples of residues that exhibit significant chemical shift perturbation during the course of titrating unlabeled HPr into $^{15}$N-labeled EIN (Glu-83 in helix α2′ and Gly-134 in helix α4) and unlabeled EIN into $^{15}$N-labeled HPr (Ser-43 in strand β3 and Leu-50 in helix α2) are shown in Fig. 4. Similar titration behavior is observed, whether the complex is biphosphorylated (*right-hand panels* in Fig. 4) or unphosphorylated (*left-hand panels* in Fig. 4) (39). The only exceptions in the chemical shift perturbation map are Gly[110] and Gln[111] located in helix α3 of EIN, which exhibit sizeable chemical shift perturbations only in the unphosphorylated complex.

$^1D_{NH}$ RDCs were measured for the biphosphorylated EIN·HPr complex using phage *pf1* as an alignment medium. Although free HPr is not compatible with *pf1*, once complexed to EIN, unduly strong interactions between HPr and *pf1* are precluded, since the positively charged binding face of HPr is buried at the interface of the EIN·HPr complex (28). (Note that the PEG/hexanol alignment medium, however, is not suitable, since it
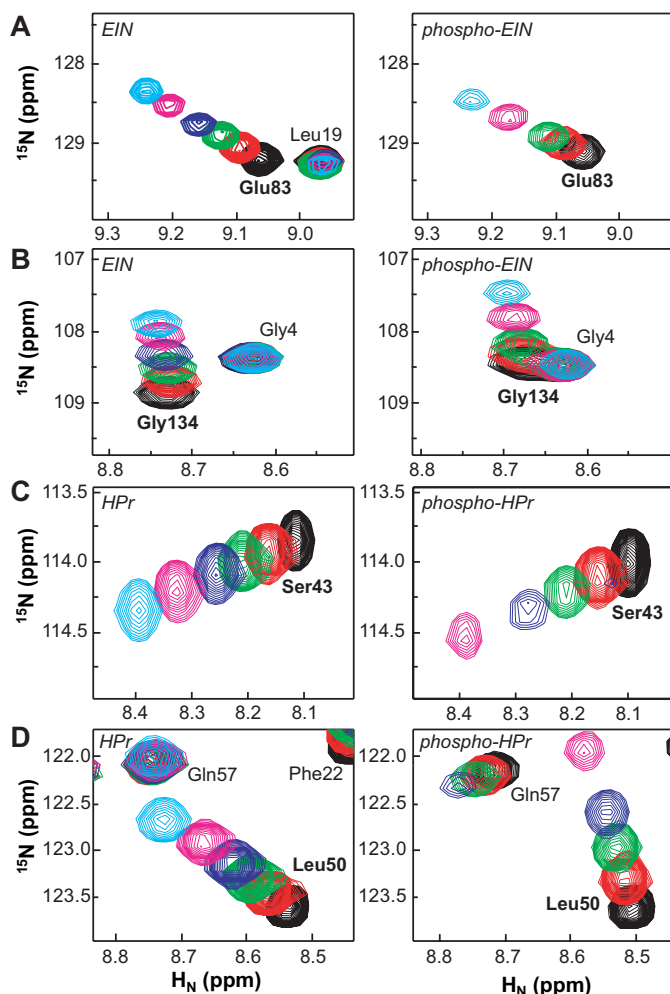


FIGURE 4. **Titration of HPr into EIN and *vice versa*, illustrating progressive chemical shift perturbation of selected cross-peaks in the $^1H$-$^{15}N$ HSQC spectra during the course of formation of unphosphorylated (*left-hand panels*) and biphosphorylated (*right-hand panels*) EIN·HPr complexes.** *A* and *B*, titration of unlabeled HPr into $^{15}$N-labeled EIN; *C* and *D*, titration of unlabeled EIN into $^{15}$N-labeled HPr. The molar ratios are *color-coded* as follows: 0 (*black*), 0.1 (*red*), 0.2 (*green*), 0.3 (*blue*), 0.5 (*magenta*), and 1.0 (*cyan*). The continual shift in the cross-peak positions during the course of the titrations indicates that exchange is fast on the chemical shift time scale for the formation of both unphosphorylated and biphosphorylated complexes.

interacts with EIN both free and complexed to HPr). The magnitude and orientation of the alignment tensors obtained by SVD using the A state coordinates of the unphosphorylated EIN·HPr complex (Protein Data Bank code 3EZA) (28) (Fig. 5A, *left*) are the same within experimental error for the global fits to EIN plus HPr and to the α and αβ domains of EIN plus HPr as for the individual fits to EIN, HPr, the α domain plus HPr, and the αβ domain (Table 3). Likewise the RDC *R*-factors for the global and individual SVD fits using the A state orientation of the α and αβ domains are comparable, ranging from 15 to 18% (Fig. 5, *B–D*). In contrast, when SVD analysis is carried out using the B state orientation of the α and αβ domains of EIN (Fig. 5A, *right*), the orientation of the alignment tensor for the α domain plus HPr is different from that for the αβ domain (Table 3), and the global fit for the α and αβ domains plus HPr is extremely poor, with an RDC *R*-factor of 63% (Fig. 5E and Table 3). Thus, one can conclude that the relative orientation of
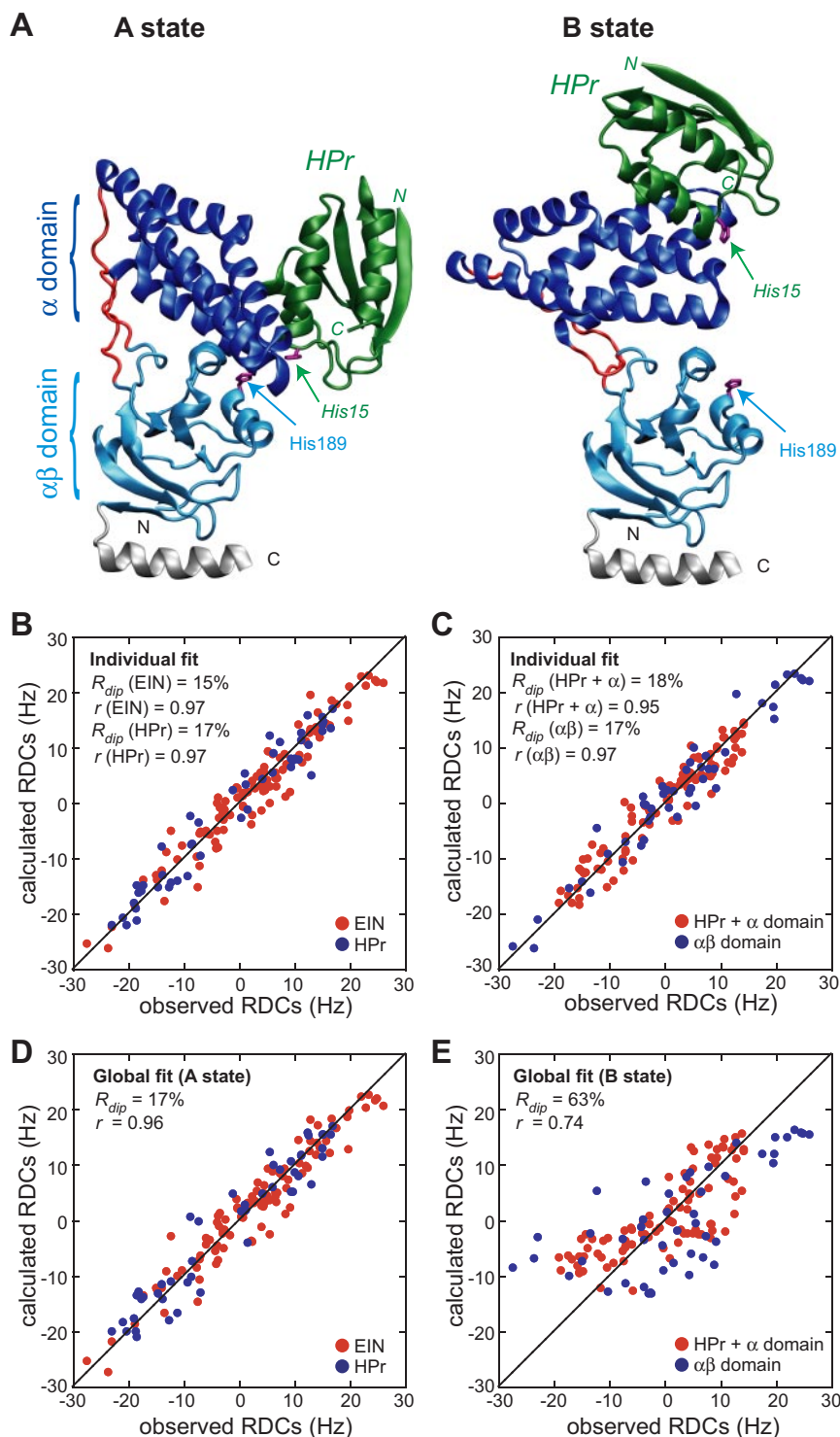
FIGURE 5. **RDC analysis of the biphosphorylated phospho-EIN·phospho-HPr complex.** *A, ribbon diagrams* of the A (*left*) and B (*right*) states of EIN complexed to HPr. The $\alpha\beta$ domains of the A and B states are shown in identical views. The $\alpha$ domain is in *dark blue*, the $\alpha\beta$ domain in *light blue*, the linkers between the $\alpha$ and $\alpha\beta$ domains in *red*, the linker helix that connects EIN to EIC in *gray*, HPr in *green*, and His-189 of EIN and His-15 of HPr in *magenta*. The C$\alpha$-C$\alpha$ distance between the active site histidines, His-189 and His-15, is 12 Å in the A state and 30 Å in the B state. The A state of EIN is taken from the NMR coordinates of the unphosphorylated EIN·HPr complex (28) (Protein Data Bank code 3EZA); the B state of EIN is taken from the x-ray coordinates of full-length phosphorylated EI (31) (Protein Data Bank code 2HWG); the binding site for HPr on the $\alpha$ domain is fully accessible in the B state, and the relative orientation of HPr to the $\alpha$ domain is taken to be the same in the A and B states. Shown is a comparison of observed (measured in an alignment medium of phage *pf1*) and calculated $^1D_{NH}$ RDCs obtained from fits to the coordinates of EIN (*red*) and HPr (*blue*) individually (*B*), fits to the coordinates of the $\alpha$ domain plus HPr (*red*) and the $\alpha\beta$ domain (*blue*) individually (*C*), a global fit to the A state using the coordinates of the unphosphorylated EIN·HPr complex (*D*), and a global fit to the B state (using the NMR coordinates of the $\alpha$ domain plus HPr and the $\alpha\beta$ domain best fitted onto the x-ray coordinates of the $\alpha$ and $\alpha\beta$ domains, respectively, of phosphorylated EI) (*E*). The values of the correlation coefficients and RDC *R*-factors are shown, and the five parameters describing the orientation and magnitude of the alignment tensors are given in Table 3.

**TABLE 3**

SVD analysis of $^1D_{NH}$ RDCs measured for the biphosphorylated phospho-EIN·phospho-HPr complex

| | Number of RDCs | Euler angles | | | $D_a^{NH}$ | $\eta$ | RDC R-factor |
| --- | --- | --- | --- | --- | --- | --- | --- |
| | | $\varphi$ | $\theta$ | $\psi$ | | | |
| | | *degrees* | | | *Hz* | | % |
| **A state of EIN (3EZA)**[a,b] | | | | | | | |
| Individual fits | | | | | | | |
| EIN | 105 | 150 | 88 | 163 | −13.6 | 0.51 | 15.1 |
| HPr | 48 | 155 | 82 | 164 | −13.3 | 0.41 | 16.8 |
| $\alpha$(EIN) + HPr | 95 | 153 | 85 | 162 | −12.0 | 0.44 | 17.7 |
| $\alpha\beta$(EIN) | 47 | 152 | 89 | 163 | −13.6 | 0.53 | 16.7 |
| Global fit | | | | | | | |
| EIN + HPr | 153 | 152 | 86 | 163 | −13.9 | 0.49 | 17.0 |
| $\alpha + \alpha\beta$ + HPr | 142 | 152 | 87 | 162 | −12.9 | 0.50 | 18.1 |
| **B state of EIN (from 2HWG orientation)**[b,c] | | | | | | | |
| Individual fits | | | | | | | |
| $\alpha$(EIN) + HPr | 95 | 36 | 78 | 142 | −12.0 | 0.44 | 17.7 |
| $\alpha\beta$(EIN) | 47 | 152 | 89 | 163 | −13.6 | 0.53 | 16.7 |
| Global fit | | | | | | | |
| $\alpha + \alpha\beta$ + HPr | 142 | 68 | 156 | 25 | 8.4 | 0.47 | 62.6 |

[a] When using the coordinates of the unphosphorylated EIN·HPr complex (Protein Data Bank code 3EZA) (28), the magnitude ($D_a^{NH}$ and $\eta$) and orientation (Euler angles) of the alignment tensor are the same within experimental error when the RDC data are best fitted to the coordinates of EIN individually, HPr individually, the $\alpha$ domain (residues 33–143) of EIN plus HPr, the $\alpha\beta$ domain (residues 2–20 and 148–230) of EIN individually, EIN plus HPr globally, and the $\alpha$ and $\alpha\beta$ domains of EIN plus HPr globally. These results indicate that the relative orientation of the $\alpha$ and $\alpha\beta$ domains of EIN and the relative orientation of EIN and HPr in the biphosphorylated complex are the same as that in the NMR structure of the unphosphorylated complex (Protein Data Bank code 3EZA), where EIN is in the A state.

[b] The molecular frame for the $\alpha\beta$ domain is the same in the calculations using the A and B state conformations of EIN.

[c] When the coordinates of the $\alpha$-domain plus HPr and the $\alpha\beta$ domain taken from the 3EZA coordinates are best fitted individually onto the coordinates of the $\alpha$ and $\alpha\beta$ domains, respectively, from the crystal structure of phosphorylated EI (31) (Protein Data Bank code 2HWG) to obtain the B state relative orientation of the $\alpha$ and $\alpha\beta$ domains, it is apparent that the orientation of the alignment tensor for the $\alpha$ domain plus HPr is different from that of the $\alpha\beta$ domain, and that the global fit for the $\alpha$ and $\alpha\beta$ domains plus HPr does not agree with the RDC data (RDC R-factor 62.6%). These data prove that the orientation of the $\alpha$ and $\alpha\beta$ domains of EIN adopted in the biphosphorylated EIN·HPr complex is different from that observed in the 2HWG crystal structure of phosphorylated EI (B state).
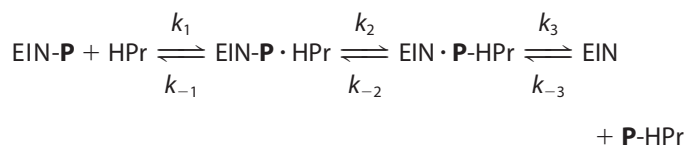
EIN and HPr and the orientation of the $\alpha$ and $\alpha\beta$ domains of EIN are the same in the unphosphorylated (28) and biphosphorylated complexes.

Since both chemical shift perturbation and RDC measurements indicate that the unphosphorylated and biphosphorylated EIN·HPr complexes have very similar binding interfaces and orientations, it is likely that the difference observed for the chemical shift perturbation of Gly-110 and Gln-111 of EIN originates from a localized alteration in a side chain conformer. The most likely candidate is the aromatic ring Phe-48 of HPr, which is in close spatial proximity to both Gly-110 and Gln-111 in the unphosphorylated complex structure (28); a small change in the position of the aromatic ring of Phe-48 would result in a concomitant alteration in ring current shifts and could easily account for the absence of any significant perturbation of the backbone amide resonances of Gly-110 and Gln-111 in the biphosphorylated complex.

*Phosphotransfer Reaction Rate*—The overall phosphoryl transfer reaction rate between EIN and HPr was monitored by recording a series of $^1H$-$^{15}N$ HSQC spectra subsequent to depletion of PEP, as described in Ref. 40. In the presence of catalytic amounts of EI and excess PEP, both proteins are fully phosphorylated. At the point where all PEP is consumed, both EIN and HPr are therefore fully phosphorylated. After about

2.5 h post-PEP depletion, both proteins are fully dephosphorylated. At intermediate time points, the solution comprises a mixture of biphosphorylated, monophosphorylated, and unphosphorylated EIN·HPr complexes. Under these conditions, the line widths of cross-peaks in the $^1H$-$^{15}N$ HSQC spectrum will be influenced by the overall rate of phosphoryl transfer within the monophosphorylated complex, depending on the chemical shift difference between the phosphorylated and unphosphorylated states of the proteins and the population of the monophosphorylated complex.

The reversible phosphoryl transfer reaction can be described by three reversible steps as depicted in Scheme I,

$$\text{EIN-}\mathbf{P} + \text{HPr} \underset{k_{-1}}{\overset{k_1}{\rightleftharpoons}} \text{EIN-}\mathbf{P} \cdot \text{HPr} \underset{k_{-2}}{\overset{k_2}{\rightleftharpoons}} \text{EIN} \cdot \mathbf{P}\text{-HPr} \underset{k_{-3}}{\overset{k_3}{\rightleftharpoons}} \text{EIN}$$
$$+ \mathbf{P}\text{-HPr}$$

SCHEME 1

where **P** denotes the phosphoryl group and the chemical point denotes the complex state. The first and third steps in scheme I are binding events that are in fast exchange on the chemical shift time scale (*cf.* Fig. 4). The second step represents the first order phosphoryl transfer reaction in the monophosphorylated complex. To estimate the overall rate constant for phosphoryl transfer, given by $k_{ex} = k_2 + k_{-2}$, residues were selected that exhibit $^1H_N$/$^{15}N$ chemical shift changes only upon phosphorylation but no perturbation upon binding. Thus, the only exchange contribution to the line widths of the $^1H_N$/$^{15}N$ cross-peaks for these residues arises from phosphoryl transfer between the proteins and not from binding. Note that loss of the phosphoryl group to solvent by hydrolysis is slow ($t_{1/2} \sim 20$ min) on the chemical shift time scale and therefore does not result in any exchange contribution to the line widths.

To this end, we selected the $^1H_N$/$^{15}N$ cross-peaks of Leu-158, Lys-175, Gly-178, and Gly-204 of EIN, all of which are located far away from the HPr binding interface in the complex and do not titrate upon the addition of HPr (Fig. 6). The observed NMR signals arise predominantly from the complex states (>90%), since the concentrations (1 mM) of EIN and HPr used are much higher than the equilibrium dissociation constants. The chemical shifts of Leu-158 and Lys-175 progressively shift during the course of the reaction from their positions in the fully phosphorylated state at time 0 (the point of PEP depletion) to those in the fully unphosphorylated state. This is the fast exchange regime on the chemical shift time scale. The differences in chemical shifts between phosphorylated and unphosphorylated states give $\Delta\omega_{HN}$ values of 311 and 399 s$^{-1}$, for Leu-158 (Fig. 6A) and Lys-175 (Fig. 6B), respectively, placing a lower limit of ~800 s$^{-1}$ on $k_{ex}$. $\Delta\omega_{HN}$ for Gly-204 (Fig. 6D) is larger, 798 s$^{-1}$, and although its cross-peak also shows a progressive shift during the course of the reaction, severe broadening is apparent in the spectra recorded between 60 and 90 min (*green contours*) and between 90 and 120 min (*blue contours*). This behavior is characteristic of an exchange process that is just on the fast side of intermediate exchange ($k_{ex} \sim \Delta\omega_{HN}$). $\Delta\omega_{HN}$ for Gly-178 is slightly larger still, 855 s$^{-1}$, and the intermediate exchange con-
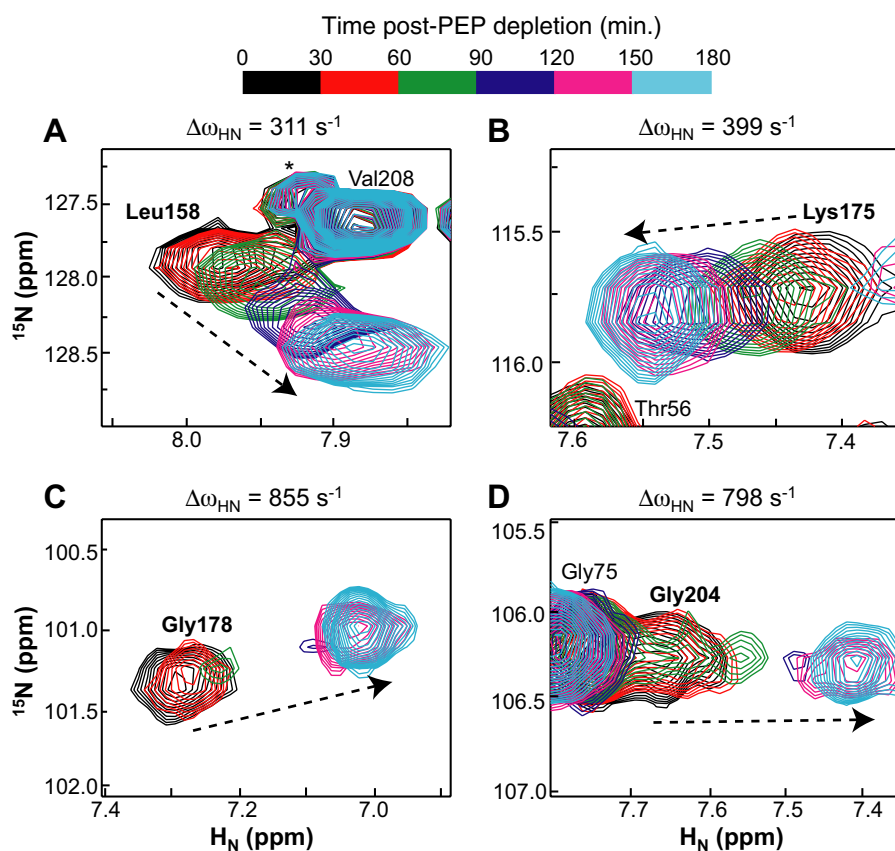
FIGURE 6. **Time course of selected cross-peaks in the $^1H$-$^{15}N$ HSQC spectra recorded during the course of active phosphoryl transfer between EIN and HPr.** Each spectrum was recorded over a period of 30 min. The zero time point is the point at which complete depletion of PEP has occurred and reflects the state in which both EIN and HPr are fully phosphorylated. The spectra are *color-coded* as follows: 0–30 min (*black*), 30–60 min (*red*), 60–90 min (*green*), 90–120 min (*blue*), 120–150 min (*magenta*), and 150–180 min (*cyan*). The last time point (*cyan*; 150–180 min post-PEP depletion) represents the spectrum of fully dephosphorylated EIN. The effects of chemical exchange arising from reversible phosphoryl transfer between EIN and HPr in the monophosphorylated EIN·HPr complex are apparent in the spectra recorded at intermediate times. The cross-peaks of Leu-158 (*A*) and Lys-176 (*B*) display fast exchange behavior with a progressive shift in cross-peak positions, whereas the behavior of the cross-peaks of Gly-178 (*C*) and Gly-204 (*D*) are characteristic of intermediate exchange in which the cross-peaks are broadened out (and in the case of Gly-178, almost beyond detection) at the time points (60–120 min) when the concentration of monophosphorylated complex is at a maximum. The direction of the cross-peak shift from the beginning to the end of the phosphotransfer reaction is indicated by the *arrows*. The cross-peaks of Leu-158, Lys-175, Gly-178, and Gly-204 are labeled in *boldface type*; cross-peaks in the same spectral window that have the same chemical shifts in the biphosphorylated and unphosphorylated EIN·HPr complex are also labeled (Val-208, Thr-56, and Gly-75 in *A*, *B*, and *D*, respectively); the cross-peak indicated by an *asterisk* in *A* is unassigned.

from the B state observed in a crystal structure of full-length phosphorylated EI that captures an intermediate corresponding to in-line autophosphorylation of His-189 by PEP bound to the EIC domain (31). In the B state, not only is His-189 buried at the interface between the $\alpha\beta$ subdomain of EIN and EIC, but it is also located ~30 Å away from His-15 HPr when HPr is docked to its binding site on the $\alpha$ subdomain (Fig. 5A, *right*). Although full-length EI is dimeric, dimerization involves exclusively the EIC (PEP-binding) domain and does not impact *per se* the configurational space available to the $\alpha$ and $\alpha\beta$ domains of EIN (31). The latter is determined by the linker regions connecting the $\alpha$ and $\alpha\beta$ subdomains (shown in *red* in Fig. 5A) and the linker helix (shown in *gray* in Fig. 5A) connecting the $\alpha\beta$ subdomain to EIC. The driving force for the interconversion of the A and B states must depend upon the strength of the interaction between the $\alpha\beta$ subdomain and EIC, which is modulated by PEP. Indeed, RDC data on full-length EI in the absence of ligand indicate that the orientation of the $\alpha$ and $\alpha\beta$ domains corresponds to the A state.[3]

Phospho-EIN and phospho-HPr can still interact with one another, albeit at reduced affinity relative to the unphosphorylated proteins, and moreover, the binding interface and relative orientation for EIN and HPr are essentially the same in the unphosphorylated and biphosphorylated complexes. The absence of any significant conformational change in the active site loop of HPr upon phosphorylation facilitates rapid phosphoryl transfer from EIN to the A domain of the sugar permease via the intermediary of HPr, thereby ensuring a rapid response to the presence of sugar in the external environment. In this regard, the unusually large, apparent bimolecular rate constants for the phosphotransfer reactions between EI and HPr ($2 \times 10^8$ $M^{-1}$ $s^{-1}$ for the transfer from EI to HPr and $4 \times 10^6$ $M^{-1}$ $s^{-1}$ for the reverse reaction) derived from transient rapid quench experiments (41) are fully consistent with the absence of any significant backbone conformational changes.

With estimates of 5 and 50 $\mu M$ for the cellular concentrations of EI and HPr, respectively (42), and a measured $K_D$ of 123 $\mu M$ (at 150 m$M$ NaCl) for the binding of phospho-EI to phospho-

dition pertains; the cross-peak appears largely at its position in either the phosphorylated (start of the reaction) or unphosphorylated states (end of the reaction), and at intermediate times between 60–120 min, the cross-peak is barely visible and broadened almost beyond the limits of detection (Fig. 6C). Thus, $k_{ex}$ is ~850 $s^{-1}$, a value that is similar to the value of 1000 $s^{-1}$ for phosphoryl transfer between the A and B domains of the mannitol transporter, Enzyme II$^{Mtl}$ (40).

*Conclusions*—In this paper, we have investigated the impact of phosphorylation on the structures of EIN and HPr and on their interaction. Phosphorylation of EIN and HPr causes no observable change in their individual backbone conformations and does not alter the relative orientation of the $\alpha$ and $\alpha\beta$ subdomains within EIN. Thus, the conformation of phospho-EIN in solution corresponds to the A state, which is compatible with in-line phosphoryl transfer between His-189 of the $\alpha\beta$ subdomain and His-15 of HPr (*cf.* Fig. 5A, *left*). The A state is distinct

---

[3] J.-Y. Suh and G. M. Clore, unpublished data.

HPr (Table 2), one can calculate that in the resting state of the PTS (*i.e.* conditions of full phosphorylation) ∼70% of phospho-EI will be in the free form. When sugar translocation turns on the PTS, HPr transfers its phosphoryl group to Enzyme II, and dephosphorylated HPr can readily bind to and accept a phosphoryl group from phospho-EI, since the affinity of the phospho-EI·HPr complex is at least 50-fold higher than that of the phospho-EI·phospho-HPr complex (*cf.* Table 2). Immediate communication between EI (PEP utilizer and cellular response regulator) and EII (sugar transporter) with HPr acting as a phosphorelay between the two proteins is key to PTS function. Modulating binding affinity between EI and HPr by phosphorylation without any significant conformational changes provides the simplest means of achieving effective and rapid signal transduction within the PTS. The weaker affinity of phospho-HPr for unphosphorylated EI compared with that of unphosphorylated HPr for phospho-EI (Table 2) allows for accumulation of unphosphorylated EI in the cell, which in turn can immediately elicit chemotactic migration toward nutrient by binding to and inhibiting autophosphorylation of CheA, a key component of the chemotaxis signaling pathway (43, 44).

## REFERENCES

1. Meadow, N. D., Fox, D. K., and Roseman, S. (1990) *Annu. Rev. Biochem.* **59,** 497–542
2. Robillard, G. T., and Broos, J. (1999) *Biochim. Biophys. Acta* **1422,** 73–104
3. Siebold, C., Flükiger, K., Beutler, R., and Erni, B. (2001) *FEBS Lett.* **504,** 104–111
4. Deutscher, J., Francke, C., and Postma, P. W. (2006) *Microbiol. Mol. Biol. Rev.* **70,** 939–1031
5. Weigel, N., Kikizurinska, M. A., Nakazawa, A., Waygood, E. B., and Roseman, S. (1982) *J. Biol. Chem.* **257,** 14477–14491
6. Garrett, D. S., Seok, Y. -J., Peterkofsky, A., Clore, G. M., and Gronenborn, A. M. (1998) *Protein Sci.* **7,** 789–793
7. Wiegel, N., Powers, D. A., and Roseman, S. (1982) *J. Biol. Chem.* **257,** 14499–14509
8. Licalsi, C., Crocenzi, T. S., Freiere, E., and Roseman, S. (1991) *J. Biol. Chem.* **266,** 19519–19527
9. Lee, B. R., Lecchi, P., Lannell, L., Jaffe, H., and Peterkofsky, A. (1994) *Arch. Biochem. Biophys.* **312,** 121–124
10. Tanaka, Y., Kimata, K., and Aiba, H. (2000) *EMBO J.* **19,** 5344–5352
11. Nam, T. W., Cho, S. H., Shin, D., Kim, J. H., Jeong, J. Y., Lee, J. H., Roe, J. H., Peterkofsky, A., Kang, S. O., Ryu, S., and Seok, Y. J. (2001) *EMBO J.* **20,** 491–498
12. Bax, A., Kontaxis, G., and Tjandra, N. (2001) *Methods Enzymol.* **339,** 127–174
13. Prestegard, J. H., Bougault, C. M., and Kishore, A. L. (2004) *Chem. Rev.* **104,** 3519–3540
14. Reddy, P., Fredd-Kuldell, N., Liberman, E., and Peterkofsky, A. (1991) *Protein Expression Purif.* **2,** 179–187
15. Delaglio, F., Grzesiek, S., Vuister, G. W., Zhu, G., Pfiefer, J., and Bax, A. (1995) *J. Biomol. NMR* **6,** 277–293
16. Garrett, D. S., Powers, R., Gronenborn, A. M., and Clore, G. M. (1991) *J. Magn. Reson.* **95,** 214–220
17. Johnson, B. A., and Blevins, R. A. (1994) *J. Biomol. NMR* **4,** 603–614
18. Clore, G. M., and Gronenborn, A. M. (1991) *Ann. Rev. Biophys Biophys. Chem.* **20,** 29–63
19. Grzesiek, S., and Bax, A. (1993) *Acc. Chem. Res.* **26,** 131–138
20. Clore, G. M., Starich, M. R., and Gronenborn, A. M. (1998) *J. Am. Chem. Soc.* **120,** 10571–10572
21. Hansen, M. R., Mueller, L., and Pardi, A. (1998) *Nat. Struct. Biol.* **8,** 1065–1074
22. Ruckert, M., and Otting, G. (2000) *J. Am. Chem. Soc.* **122,** 7793–7797
23. Schwieters, C. D., Kuszewski, J., and Clore, G. M. (2006) *Progr. Nucl. Magn. Reson. Spect.* **48,** 47–62
24. Gassner, M., Stehlik, D., Schrecker, O., Hengstenberg, W., Maurer, W., and Ruterjans, H. (1977) *Eur. J. Biochem.* **75,** 287–296
25. Dooijewaard, G., Roossien, F. F., and Robillard, G. T. (1979) *Biochemistry* **18,** 2996–3001
26. van Nuland, N. A. J., Boelens, R., Scheek, R. M., and Robillard, G. T. (1995) *J. Mol. Biol.* **246,** 180–193
27. Jones, B. E., Rajagopal, P., and Klevit, R. E. (1997) *Protein Sci.* **7,** 2107–2119
28. Garrett, D. S., Seok, Y. J., Peterkofsky, A., Gronenborn, A. M., and Clore. G. M. (1999) *Nature Struct. Biol.* **6,** 166–173
29. Garrett, D. S., Seok, Y. J., Liao, D. I., Peterkofsky, A., Gronenborn, A. M., and Clore, G. M. (1997) *Biochemistry* **36,** 2517–2530
30. Liao, D. I., Silverton, E., Seok, Y. J., Lee, B. R., Peterkofsky, A., and Davies, D. R. (1996) *Structure* **4,** 861–872
31. Teplyakov, A., Lim, K., Zhu, P. P., Kapadia, G., Chen, C. C. H., Schwartz, J., Howard, A., Reddy, P. T., Peterkofsky, A., and Herzberg, O. (2006) *Proc. Natl. Acad. Sci. U. S. A.* **103,** 16218–16223
32. Clore, G. M., and Garrett, D. S. (1999) *J. Am. Chem. Soc.* **121,** 9008–9012
33. Cornilescu, G., Lee, B. R., Cornilescu, C., Wang, G., Peterkofsky, A., and Clore, G. M. (2002) *J. Biol. Chem.* **277,** 42289–42298
34. Williams, D. C., Cai, M., Suh, J. Y., Peterkofsky, A., and Clore, G. M. (2005) *J. Biol. Chem.* **280,** 20775–20784
35. Williams, D. C., Cai, M., and Clore, G. M. (2004) *J. Biol. Chem.* **279,** 1449–1457
36. Williams, D. C., Lee, J. Y., Cai, M., Bewley, C. A., and Clore, G. M. (2005) *J. Biol. Chem.* **280,** 29269–29276
37. Jia, Z., Quail, J. W., Waygood, E. B., and Delbaere, L. T. (1993) *J. Biol. Chem.* **268,** 22490–22501
38. Suh, J. Y., Tang, C., and Clore, G. M. (2007) *J. Am. Chem. Soc.* **129,** 12954–12955
39. Garrett, D. S., Seok, Y.-J., Peterkofsky, A., Clore, G. M., and Gronenborn, A. M. (1997) *Biochemistry* **36,** 4393–4398
40. Suh, J. Y., Iwahara, J., and Clore, G. M. (2007) *Proc. Natl. Acad. Sci. U. S. A.* **104,** 3153–3158
41. Meadow, N. D., Mattoo, R. L., Savtchenko, R. S., and Roseman, S. (2005) *Biochemistry* **44,** 12790–12796
42. Rohwer, J. M., Meadow, N. D., Roseman, S., Westerhoff, H. V., Postma, P. W. (2000) *J. Biol. Chem.* **275,** 34909–34921
43. Lux, R., Jahreis, K., Bettenbrock, K., Parkinson, J. S., and Lengeler, J. W. (1995) *Proc. Natl. Acad. Sci. U. S. A.* **92,** 11583–11587
44. Lux, R., Munasinghe, R. N., Castellano, F., Lengeler, J. W., Corrie, J. E. T., and Khan, S. (1999) *Mol. Biol. Cell* **10,** 1133–1146